INTERNATIONAL JOURNAL OF HYDROGEN ENERGY 34 (2009) 8964–8973

Available at www.sciencedirect.com

ScienceDirect

journal homepage: www.elsevier.com/locate/he

Pressure loss reduction in hydrogen pipelines by surface restructuring

Y. Peet [a,*], P. Sagaut [a], Y. Charron [b]

[a] Insitut Jean Le Rond d'Alembert, UMR CNRS 7190, Université Pierre et Marie Curie – Paris 6, 4 place Jussieu - case 162, F-75252 Paris Cedex 5, France

[b] IFP- Institut Français du Pétrole, Rueil Malmaison Cedex, 92852, France

ARTICLE INFO

Article history:
Received 2 May 2009
Received in revised form
14 August 2009
Accepted 14 August 2009
Available online 18 September 2009

Keywords:
Hydrogen
Pipeline transportation
Pressure loss reduction
Structured surfaces
Turbulence

ABSTRACT

This paper concerns the reduction of pressure losses during pipeline hydrogen transportation, as the cost of hydrogen compression is a significant obstacle for efficient hydrogen pumping on a large-scale basis. The use of organized micro-structures on pipeline walls is proposed to obtain lower values of pressure losses with respect to smooth walls. Three-dimensional micro-structures of a sinusoidal shape are investigated as potentially more efficient counterparts to conventional two-dimensional structures (riblets) developed in aerospace industry. Aerodynamic performance of three-dimensional structures is investigated computationally in terms of both skin friction and pressure drag, two constituents of the total drag. Three-dimensional structures are shown to provide larger total drag reduction than two-dimensional structures for some range of geometrical parameters (14.5% versus 11%). Parametric dependence of both pressure and skin friction drag on structure geometry is analyzed, and an optimum configuration maximizing the total drag reduction is proposed.

1. Introduction

Hydrogen economy requires an infrastructure to deliver hydrogen from the production site to the point of end-use, such as a dispenser at a refueling station or stationary power site. Pipeline transmission of gaseous hydrogen is so far the most economical method for hydrogen delivery at large volumes. But due to the relatively low volumetric energy density of hydrogen, the costs associated with hydrogen compression are large. Reduction of pressure losses in pipes would decrease the number of compression stations along the pipe and lower the costs associated with the pipeline hydrogen delivery.

More than three decades ago, hydrogen was recognized as a promising alternative energy source, and researchers started looking into many issues related to hydrogen economy, such as methods of hydrogen production, storage and transportation, including pipeline transmission, with the review of early studies published, for example, by Gregory & Pangborn [1]. Later, Tellier [2] proposed to use axial flow compressors, as opposed to centrifugal compressors, for long distance pipeline transmission of hydrogen. Energy losses associated with pipeline transmission of liquid hydrogen were studied in [3], and technical and economical evaluation of pipeline transportation of gaseous hydrogen was presented in [4]. The authors of [4] showed that it is economically feasible to transport hydrogen or hydrogen–natural gas mixtures over long distances under the conditions of high production pressures and large markets. Since then, many various aspects associated with pipeline transmission of gaseous hydrogen were investigated, including safety implications [5–7], choice

* *Corresponding author*. Tel.: +1 847 491 7243.
E-mail address: peet@lmm.jussieu.fr (Y. Peet).

0360-3199/$ – see front matter
doi:10.1016/j.ijhydene.2009.08.035

of pipeline materials and problem of hydrogen embritllement [8,9], modeling and optimization of hydrogen networks based on dynamic programming methods [10], neuronal networks [11] and geographical information systems [12]. Computational modeling of a hydrogen gas flow inside the pipelines was undertaken by Weng & Zhen [13] and Elaoud & Hadj-Taieb [14]. However, the aspect of pressure loss reduction in gas hydrogen pipelines was not extensively considered in the open literature.

In a gas pipeline, pressure losses are mostly defined by the flow conditions and by the characteristics of the pipe wall in contact with the gas. In a first stage, pressure losses may be reduced by using a relatively smooth internal coating, which decreases wall roughness and therefore decreases a friction factor. In a second stage, pressure losses can be further reduced by using structured surfaces on a coated pipe. Structured surfaces favorably interact with the turbulent boundary layer on the pipe wall, decreasing the momentum transfer associated with the most energetic turbulent structures and thus decreasing the friction factor relative to a smooth wall [15–17]. It was estimated [18] that, for a pipeline operating at a pressure of 150 bar, reducing the wall roughness from 20 to 2 microns provides a cost saving of 11–12%, depending on a discharge pressure. Addition of structured surfaces, which can be represented by negative roughness, provides 16–17% costs saving (for structured surfaces designed for 5–10% drag reduction), which gives an extra 5–6% gain relative to a coating with 2 micron roughness. Although structured surfaces can also be used with application to natural gas, they are especially well suited for use with hydrogen for two reasons. First, due to a higher purity of hydrogen, erosion of structured surfaces leading to a decrease or complete loss of drag reduction efficiency is less likely to occur. Second, since molecular weight and, therefore, density (ρ) of hydrogen is about ten times smaller than that of natural gas while viscosities (μ) are similar, the Reynolds number $Re = \rho\, UD/\mu$ of hydrogen is also about ten times smaller than that of natural gas at the same operating (bulk) velocity U and pipe diameter D. Since physical size of the structures is roughly proportional to the pipe diameter/Reynolds number ratio (D/Re), the structures will be ten times larger for hydrogen and, therefore, easier to manufacture. However, even for hydrogen, they will be of a size of 50–100 microns, still representing significant challenges for manufacturing. A special technique for manufacturing micro-structures on gas pipeline walls using laser ablation with pulsed lasers has been developed at IFP [18], consisting of fabrication of a primary mould, fabrication of a secondary mould from the primary mould (flexible membrane, generally silicon) and application of a flexible membrane on a coating during its polymerization stage (pressurization).

When offering structured surfaces as a viable technique for reducing pipeline pressure losses, one has to take into account the costs associated with the surface structuring. Application of structured surfaces with the laser ablation requires the manufacturing of structured bladders. Although the primary mould itself can be very costly, its cost becomes totally negligible based on a thousand kilometers of pipeline length. The cost of the mould replication and the application of a flexible membrane to the pipeline coating is of the order of the cost of a conventional coating application, which is about 6 euros/m^2, compared to 600 euros/m^2 of overall pipeline costs (which include installation, operating and maintenance costs of the piping, compression stations and utilities). In other words, costs of surface restructuring would be about 1–2% of the overall CAPEX and OPEX costs, compared to 16–17% cost savings which they can offer by reducing pressure losses.

Aerodynamic performance associated with two-dimensional (2D) structured surfaces has been extensively investigated for over 20 years, and an optimal geometry has been established experimentally providing 4–11% drag reduction depending on a cross-sectional shape [19–21]. However, drag reduction properties of structured surfaces can be further improved by designing three-dimensional (3D) structures to reinforce the turbulence control not only in normal direction, but also in transverse and longitudinal directions. Thus, it was recently proposed to add longitudinal variation to a conventional two-dimensional geometry of structures [22] in an attempt to create flow conditions similar to that occurring above a spanwise-oscillating wall, which is known to provide flow drag reduction of 15–20% when external energy input is taken into account [23–25]. The new three-dimensional structures represent sinusoidal waves, rather than straight lines, if viewed from above. This paper is devoted to a computational study of aerodynamic performance of those three-dimensional structures with respect to the two major parameters defining their longitudinal geometry: amplitude and wavelength of the sinusoidal shape oscillations. Cross-sectional shape in the transverse plane is chosen to correspond to the optimal shape of the two-dimensional structures. Two types of transverse cross-sections are considered: triangular and knife-blade. Aerodynamic performance in terms of both skin friction and pressure drag is documented, since pressure drag becomes non-zero for 3D structures as opposed to conventional 2D structures. Total drag modification with respect to the corresponding 2D configurations is assessed.

2. Geometry of the structured surfaces

Three-dimensional view of a structured surface is shown in Fig. 1. We consider two types of transverse cross-section of structures: triangular and knife-blade. The close view of each cross-section, together with the major parameters defining the cross-sectional geometry, is shown in Fig. 2. Here s is the spacing between the two adjacent structures, h is the protrusion height of the structures, and α is the protrusion angle. The angle α equals to 90° for the knife-blade cross-section. The difference between conventional two-dimensional structures and proposed three-dimensional (wavy) structures [22] is highlighted in Fig. 3, where we show the top view of the structured surface. Major parameters defining the longitudinal variation of the structure geometry due to the wavy pattern are the wavelength λ and the amplitude a (which uniquely define the maximum slope β).

In the calculations, the cross-sectional geometry of the structures was kept constant corresponding to the optimum configuration of 2D structures for this type of the cross-section. The values of the optimum cross-sectional parameters are listed in Table 1 for the triangular and knife-blade

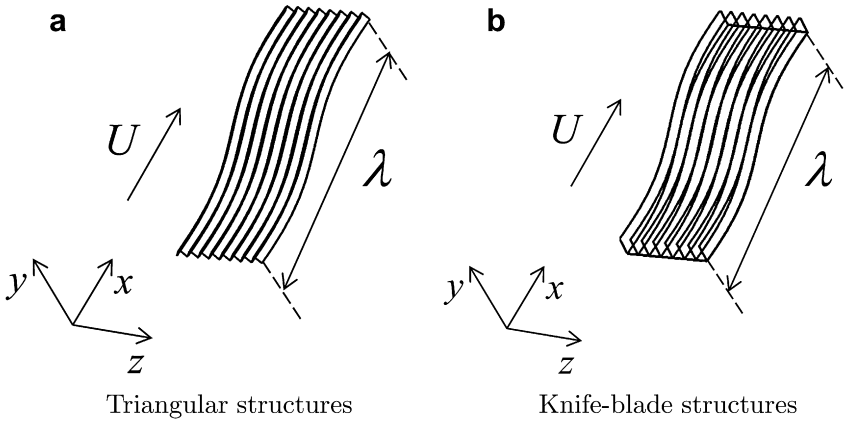

Fig. 1 – Structured surface.

cross-sections, respectively, and can be found, for example, in Ref. [21].

It is known from the analysis of governing equations and from the multitude of experimental evidence that turbulent boundary layers at different Reynolds numbers exhibit self-similarity and that the self-similar character of the near-wall turbulence is defined by special reduced units, called ''wall'' or ''plus'' units: $l^+ = l/l_\tau$, where $l_\tau = \mu/(\rho\ u_\tau)$ is the friction length and $u_\tau = \sqrt{\tau_0/\rho}$ is the friction velocity, τ_0 is the shear stress on a smooth wall [26]. It means that the major properties of turbulent boundary layers, such as the typical size of the structural sublayers in a turbulent boundary layer (viscous sublayer, logarithmic sublayer, buffer layer and external layer), as well as the characteristic size of coherent turbulent motions (coherent vortices) are the same if expressed in wall units for flows with different Reynolds numbers [26]. Therefore, wall units are typically used when analyzing turbulent boundary layers. Moreover, since the characteristic size of coherent vortices scales with wall units, so does the optimum size of drag reducing surface structures, whose purpose is to interact with these vortices and reduce the turbulent activity associated with them. Optimum parameters of the structure geometry, defined in wall units, will therefore stay the same when the Reynolds number of the flow changes, so that these parameters in wall units can be determined for one particular flow condition and be used for different flow conditions. Physical size of the structures, l, can be reconstructed from the size in wall units, l^+, following the relation $l = l^+\ D/Re_\tau$, where $Re_\tau = D/l_\tau = \rho\ u_\tau\ D/\mu$. From the empirical law of Blasius for the turbulent friction factor in smooth pipes [27],

$$F_f = 0.3164\mathrm{Re}^{-1/4}, \tag{1}$$

where the friction factor $F_f = 8\ u_\tau^2/U^2$, it follows that

$$\mathrm{Re}_\tau \sim 0.2\ \mathrm{Re}^{7/8} \tag{2}$$

and the physical size of the structures can be computed as

$$l \sim 5.l^+ D/\mathrm{Re}^{7/8}. \tag{3}$$

Therefore, the structure size is roughly proportional to the pipe diameter/Reynolds number ratio. Although only one choice concerning structure parameters can be made for a particular pipeline based on design operating conditions (gas velocity, density and viscosity), some working deviations of gas parameters from the targeted values are acceptable, since the operational range of structured surfaces is reasonably large. In fact, for changes in Reynolds number up to 50%, the performance of a structured surface, although no longer optimum, will still be sufficient to provide pressure loss reduction benefits. If operating conditions are to change significantly, as with the change of a transported fluid or pipeline infrastructure, the application of a new inner surface

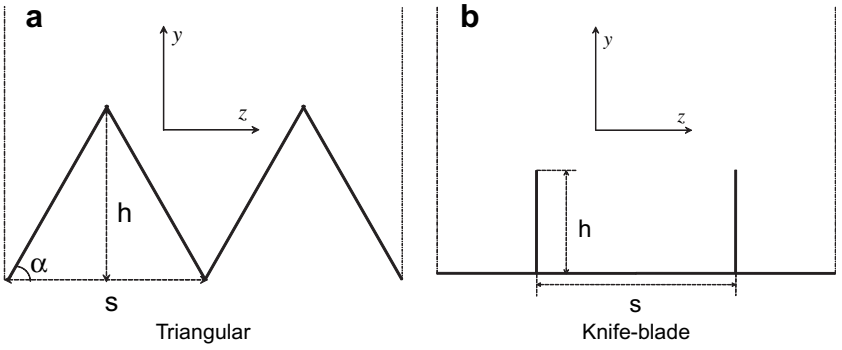

Fig. 2 – Cross-sectional geometry.

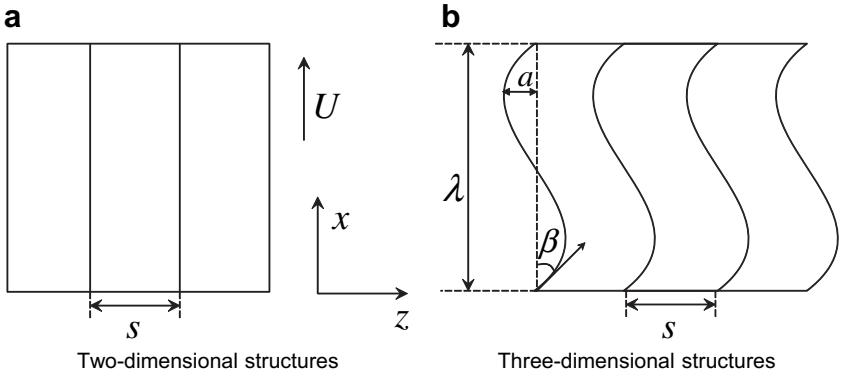

Fig. 3 – Comparison between 2D and 3D structures. Top view of the structured surface.

coating with differently-sized structures should be considered, which, as estimated above, does not constitute the major costs in renovating a pipeline infrastructure.

Since the goal of this paper is to examine the effect of longitudinal variation of structure geometry on the flow drag, several configurations involving different wavelengths and amplitudes of a sinusoidal wave defining the structure shape were tested computationally. Geometrical parameters of these configurations are summarized in Tables 2 and 3 for triangular and knife-blade cross-sections, respectively. In addition to the wavelength (λ^+) and amplitude (a^+) in wall units, as well as the slope angle β, we also report the non-dimensional period T^+ defined as $T^+ = T\ u_\tau^2/\nu$, where $T = \lambda/U$ and ν is the kinematic viscosity, and the transverse excitation parameter $a^+/T^{+\ 3}$, which will be discussed later (Section 6). The non-dimensional oscillation period is the most relevant parameter in regard to a spanwise-oscillating wall - the drag reduction mechanism that motivated the development of wavy structures. The quantity T^+ is therefore useful for direct comparison between the two drag reduction methods. In the present application, T^+ can be understood as the non-dimensional time it takes the flow to travel through one wavelength of a structure shape oscillation. Knife-blade cross-section is known to be the most efficient structure shape for reducing drag in 2D configurations [21] (10–11% drag reduction as opposed to 5–6% for triangular cross-section). It was therefore believed that the knife-blade cross-section would also be the most efficient in extracting benefits from the longitudinal geometry variation, thus providing the largest difference in drag between 3D and 2D shapes. This explains our decision to concentrate most of our efforts concerning parametric study of 3D configurations and their drag reduction properties on knife-blade structures. Although knife-blade structures with zero blade thickness cannot be used in practice (because of the low durability and manufacturing difficulty), very similar shapes, such as structures with trapezoidal grooves and thin wedge-like ribs, can be used [21].

3. Computational setup

Computations of the turbulent flow over structured surfaces were performed using *Code_Saturne* [28], which is an unstructured finite-volume incompressible computational solver of a second-order accuracy both in space and in time. Although hydrogen by itself is not an incompressible fluid and compressibility effects would be important, say, at the compressor entrance, pipeline transport operates at very small Mach numbers $M = U/c$, which, for the case of hydrogen usually do not exceed $M \sim 0.01$–0.03 due to the high value of the sound speed $c = \sqrt{(\gamma P/\rho)}$, making the flow essentially incompressible. In addition, it was recently evaluated that even at high Mach numbers $M > 1$ compressibility effects on the pressure losses in turbulent flows are negligible [29]. In the present paper, large Eddy Simulation procedure with Smagorinsky model [30] as a subgrid-scale model was used for turbulence modeling. Simulations were setup in a channel, whose bottom wall was a structured surface, and the top wall was a smooth wall, see Fig. 4. All turbulence length scales were fully resolved in streamwise and spanwise directions, while van Driest wall functions [31] were used in the vertical direction. Computational domain contained eight surface structures in the spanwise direction and its length was equal to one oscillation wavelength in the streamwise direction, while periodic boundary conditions were employed at both streamwise and spanwise boundaries. Reynolds number was set to $Re = \rho\, UD_h/\mu = 11{,}200$, where D_h is the hydraulic diameter, which, for an infinitely wide channel is calculated as $D_h = 2\,L_y$, where L_y is the

Table 1 – Cross-sectional parameters of the structure geometry.

Cross-section	α	h/s	h^+	s^+
Triangular	60°	0.866	18	21
Knife-blade	90°	0.5	8	16

Table 2 – Wave parameters for triangular cross-section.

Case	λ^+	a^+	β	T^+	$a^+/T^{+\ 3}$
2D T	∞	0	0°	∞	0
3D–70–11.3 T	1080	34	11.3°	70	1.00×10^{-4}
3D–37–11.3 T	580	18	11.3°	37	3.55×10^{-4}

Table 3 – Wave parameters for knife-blade cross-section.

Case	λ^+	a^+	β	T^+	$a^+/T^{+\,3}$
2D B	∞	0	0°	∞	0
3D–105–11.3 B	1620	50	11.3°	105	0.43×10^{-4}
3D–70–8 B	1080	23	8°	70	0.67×10^{-4}
3D–70–9.6 B	1080	28	9.6°	70	0.82×10^{-4}
3D–70–11.3 B	1080	34	11.3°	70	1.00×10^{-4}
3D–37–9.6 B	580	15	9.6°	37	2.96×10^{-4}
3D–37–20 B	580	32	20°	37	6.32×10^{-4}

channel height. This Re corresponds to Reynolds number based on skin friction velocity $Re_\tau = \rho\ u_\tau D_h/\mu = 720$. Geometrical parameters of the computational domain with respect to the hydraulic diameter D_h are summarized in Table 4 for all the computed cases. We also list the number of grid points used in each direction ($N_x \times N_y \times N_z$) and the grid resolution in wall units. The physical size of the structures with respect to the hydraulic diameter for this Reynolds number is documented in Table 5 (calculated from the non-dimensional structure parameters listed in Tables 1–3). Further details of the computational setup can be found in Refs. [32–34]. Both the domain size and the grid resolution guarantee the absence of an artificially introduced coherence and excessive damping of the organized turbulent structures in a surface boundary layer [16,35]. Present calculations were validated for the case of a plane channel flow [32] (versus Direct Numerical Simulations (DNS) of Abe et al. [36]) and for the case of a channel flow whose bottom wall was a structured surface with 2D triangular structures [33] (versus DNS of Choi et al. [16]).

4. Skin friction and pressure drag

Local force that acts on a surface at a particular point consists of shear and pressure forces

$$\vec{F} = -\left[\mu\left(\nabla\vec{v} + (\nabla\vec{v})^T\right)\Big|_w \cdot \vec{n} - P_w \cdot \vec{n}\right], \tag{4}$$

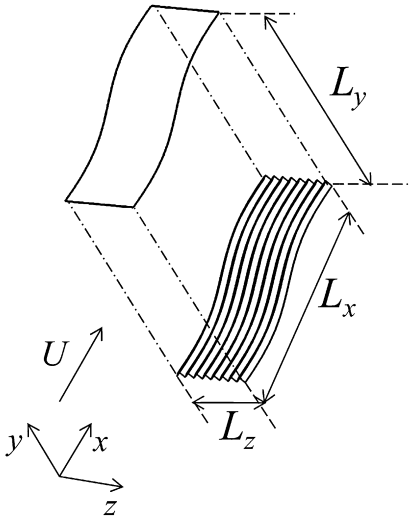

Fig. 4 – Computational domain.

where $\vec{v}$ is the velocity vector, P is the pressure, $\vec{n}$ is the outward pointing normal of the unit length, and the subscript "w" stands for the quantities evaluated at the wall. Streamwise component of the local surface force (aligned with the mean flow direction) defines the drag force

$$F_d = -\left[\mu(\nabla\vec{v} + (\nabla\vec{v})^T)|_w \cdot \vec{n} \cdot \vec{i} - P_w \cdot \vec{n} \cdot \vec{i}\right], \tag{5}$$

where $\vec{i}$ is the unit vector in the streamwise direction. Equation (5) can be further transformed into (see, for example, Ref. [34])

$$F_d = -\mu\left(\frac{\partial u}{\partial n}\right)\Big|_w + P_w \cdot n_x, \tag{6}$$

where u is the local streamwise velocity, and n_x is the streamwise component of the surface normal vector. Since $n_x = 0$ on a smooth wall (wall without surface structures), pressure drag is absent in the flow through a conventional smooth pipe, and the only contribution to the total pressure loss in a pipeline is the friction drag. Moreover, for the two-dimensional structures (Fig. 3a), n_x is also zero, and the pressure drag is again identically zero. It explains why all previous studies of the flow drag reduction with conventional (2D) structures were only concerned with the skin friction drag. For the wavy three-dimensional structures (Fig. 3b), n_x is no longer zero, and the pressure drag should be considered, together with the skin friction drag, in order to judge the overall aerodynamic performance of the structured surface.

5. Drag modification by structured surfaces

We document the values of both the skin friction and the pressure drag in terms of the surface-averaged non-dimensional coefficients, C_f and C_p, defined as

$$C_f = \frac{1}{1/2\rho U^2 S_{sm}} \iint_S -\mu\left(\frac{\partial u}{\partial n}\right)\Big|_w \mathrm{d}S, \tag{7}$$

$$C_p = \frac{1}{1/2\rho U^2 S_{sm}} \iint_S P_w n_x \,\mathrm{d}S, \tag{8}$$

as well as the total drag coefficient $C_d = C_f + C_p$ in Table 6. In the above equations, S is the wetted area of the structured surface, and S_{sm} is the corresponding area of the smooth surface. Please, note, that the skin friction coefficient defined by Eq. (7) corresponds to 1/4 of the friction factor F_f appearing in Eq. (1). Value of the drag modification with respect to the smooth surface can be defined as

$$\Delta C_d = \frac{C_d^{str} - C_d^{sm}}{C_d^{sm}}, \tag{9}$$

where C_d^{sm} is the drag coefficient of the smooth surface, and C_d^{str} is the drag coefficient of the structured surface. Since $C_p^{sm} = 0$ and, therefore, $C_d^{sm} = C_f{}^{sm}$, Eq. (9) can be further reduced to

$$\Delta C_d = \frac{C_f{}^{str} - C_f{}^{sm}}{C_f{}^{sm}} + \frac{C_p{}^{str}}{C_f{}^{sm}} = \Delta C_f + \Delta C_p. \tag{10}$$

Table 4 – Geometrical parameters of the computational domain.

Case	L_x/D_h	L_y/D_h	L_z/D_h	$N_x \times N_y \times N_z$	$\Delta x^+ \times \Delta y^+ \times \Delta z^+$
2D T	0.805	0.5	0.2328	$16 \times 64 \times 128$	$36 \times (0.4–14) \times 1.32$
3D–70–11.3 T	1.5	0.5	0.2328	$32 \times 64 \times 128$	$33 \times (0.4–14) \times 1.32$
3D–37–11.3 T	0.805	0.5	0.2328	$16 \times 64 \times 128$	$36 \times (0.4–14) \times 1.32$
2D B	0.805	0.5	0.1816	$16 \times 64 \times 128$	$36 \times (0.4–14) \times 1.03$
3D–105–11.3 B	2.25	0.5	0.1816	$48 \times 64 \times 128$	$36 \times (0.4–14) \times 1.03$
3D–70–8 B	1.5	0.5	0.1816	$32 \times 64 \times 128$	$33 \times (0.4–14) \times 1.03$
3D–70–9.6 B	1.5	0.5	0.1816	$32 \times 64 \times 128$	$33 \times (0.4–14) \times 1.03$
3D–70–11.3 B	1.5	0.5	0.1816	$32 \times 64 \times 128$	$33 \times (0.4–14) \times 1.03$
3D–37–9.6 B	0.805	0.5	0.1816	$16 \times 64 \times 128$	$36 \times (0.4–14) \times 1.03$
3D–37–20 B	0.805	0.5	0.1816	$16 \times 64 \times 128$	$36 \times (0.4–14) \times 1.03$

Values of ΔC_f, ΔC_p and ΔC_d with respect to the smooth surface are listed in Table 7.

Time history of the skin friction and total drag modification, DC_f and DC_d, is shown in Fig. 5 for triangular and knife-blade structures. From Table 7 and Fig. 5 it is seen that:

1. As expected, knife-blade structures are more efficient than triangular structures both in 2D and 3D configurations.
2. 3D structures with short wavelength ($T^+ = 37$) perform worse than 2D structures; however, 3D structures with longer wavelengths ($T^+ = 70$ and $T^+ = 105$) perform better than 2D structures.
3. Long 3D structures are able to reduce the *skin friction drag* significantly with respect to 2D structures: reduction of skin friction by half as compared to 2D structures is possible for some configurations (3D–70–11.3 T and 3D–70–11.3 B).
4. When the *total drag* is considered (skin friction drag + - pressure drag), significant reduction by at least 30% of the corresponding 2D value can still be obtained for an optimum knife-blade configuration (3D–70–11.3 B).

6. Parametric dependence

In order to design the most efficient three-dimensional structures for the drag reduction purposes, it is necessary to understand how the drag value depends on the geometrical parameters of the structure shape. Analyzing Tables 2, 3 and 6, it is easy to see that the pressure drag depends solely on the slope angle β. Indeed, if the pressure coefficient, C_p, is plotted versus tan β (Fig. 6), quadratic dependence

$$C_p \sim A(\tan\beta)^2 \tag{11}$$

is recovered, where $A \sim 5.5 \times 10^{-3}$. Since the maximum spanwise velocity attained by the fluid particles during the oscillatory motion induced by the structure shape is proportional to tan β ($w \sim U \tan\beta$), the pressure coefficient behaves like $C_p \sim A(w/U)^2$, which is in perfect agreement with the fact that the additional pressure drag in 3D structures is due to the conversion of the transverse kinetic energy.

For the skin friction drag, the parametric dependence is more complex. One needs two parameters, for example, (β, a^+), (β, λ^+), (a^+, λ^+), (a^+, T^+) etc. to completely define the oscillatory geometry of structures. From careful examination of Tables 6 and 7 it is seen that, unlike with the pressure drag, changes in the skin friction drag cannot be described by a single parameter, and it is a combination of two parameters that determines the skin friction value. Charron & Trapy [37] suggested the transverse excitation parameter,

$$\varepsilon = a^+/T^{+3}, \tag{12}$$

as the relevant parameter with respect to a skin friction modification by the oscillatory motion, since, if plotted against this parameter, skin friction reduction values were placed on a single curve with the least scatter in their calculations. The transverse excitation can be viewed as the maximum transverse acceleration reached by the fluid particles during the oscillatory motion divided by the time

Table 5 – Physical size of the structures for the given Reynolds number.

Case	s/D_h	a/D_h	λ/D_h
2D T	0	0	0
3D–70–11.3 T	0.0341	0.05	1.5
3D–37–11.3 T	0.0341	0.025	0.805
2D B	0	0	0
3D–105–11.3	0.0227	0.07	2.25
3D–70–8 B	0.0227	0.03	1.5
3D–70–9.6 B	0.0227	0.04	1.5
3D–70–11.3 B	0.0227	0.05	1.5
3D–37–9.6 B	0.0227	0.02	0.805
3D–37–20 B	0.0227	0.045	0.805

Table 6 – Skin friction, pressure and total drag coefficients for the computed cases.

Case	C_f	C_p	C_d
Smooth wall	8.80×10^{-3}	0	8.80×10^{-3}
2D T	8.32×10^{-3}	0	8.32×10^{-3}
3D–70–11.3 T	8.15×10^{-3}	0.18×10^{-3}	8.33×10^{-3}
3D–37–11.3 T	8.84×10^{-3}	0.18×10^{-3}	9.02×10^{-3}
2D B	7.81×10^{-3}	0	7.81×10^{-3}
3D–105–11.3 B	7.52×10^{-3}	0.21×10^{-3}	7.73×10^{-3}
3D–70–8 B	7.52×10^{-3}	0.11×10^{-3}	7.63×10^{-3}
3D–70–9.6 B	7.52×10^{-3}	0.17×10^{-3}	7.70×10^{-3}
3D–70–11.3 B	7.30×10^{-3}	0.21×10^{-3}	7.51×10^{-3}
3D–37–9.6 B	7.85×10^{-3}	0.14×10^{-3}	7.99×10^{-3}
3D–37–20 B	8.54×10^{-3}	0.78×10^{-3}	9.34×10^{-3}

Table 7 – Drag modification by structured surfaces with respect to the smooth wall.

Case	ΔC_f	ΔC_p	ΔC_d
2D T	−5.4%	0%	−5.4%
3D–70–11.3 T	−7.4%	+2.0%	−5.4%
3D–37–11.3 T	+0.5%	+2.0%	+2.5%
2D B	−11.2%	0%	−11.2%
3D–105–11.3 B	−14.5%	+2.4%	−12.1%
3D–70–8 B	−14.5%	+1.2%	−13.3%
3D–70–9.6 B	−14.5%	+1.9%	−12.4%
3D–70–11.3 B	−17%	+2.4%	−14.6%
3D–37–9.6 B	−10.8%	+1.6%	−9.2%
3D–37–20 B	−3.0%	+8.9%	+5.9%

required to reach this acceleration. We plot our results for the skin friction modification, ΔC_f, versus the transverse excitation parameter ϵ (values listed in Tables 2 and 3) in Fig. 7, as well as the results of the calculations of Charron & Trapy [37] performed for the knife-blade structures with the same cross-sectional shape interacting with forced turbulence (as opposed to the natural boundary layer turbulence in the present calculations), at three different Reynolds numbers. When the excitation is zero, it corresponds to the two-dimensional structures. When the excitation increases, the transverse oscillation of the mean flow velocity leads to tilting and weakening of the near-wall turbulent structures, thus reducing the turbulent momentum transfer to the wall and decreasing the skin friction. If the excitation is too large, however, the near-wall turbulence is driven from its equilibrium state, which results in a rapid growth of the skin friction. For the large values of the excitation parameter, the

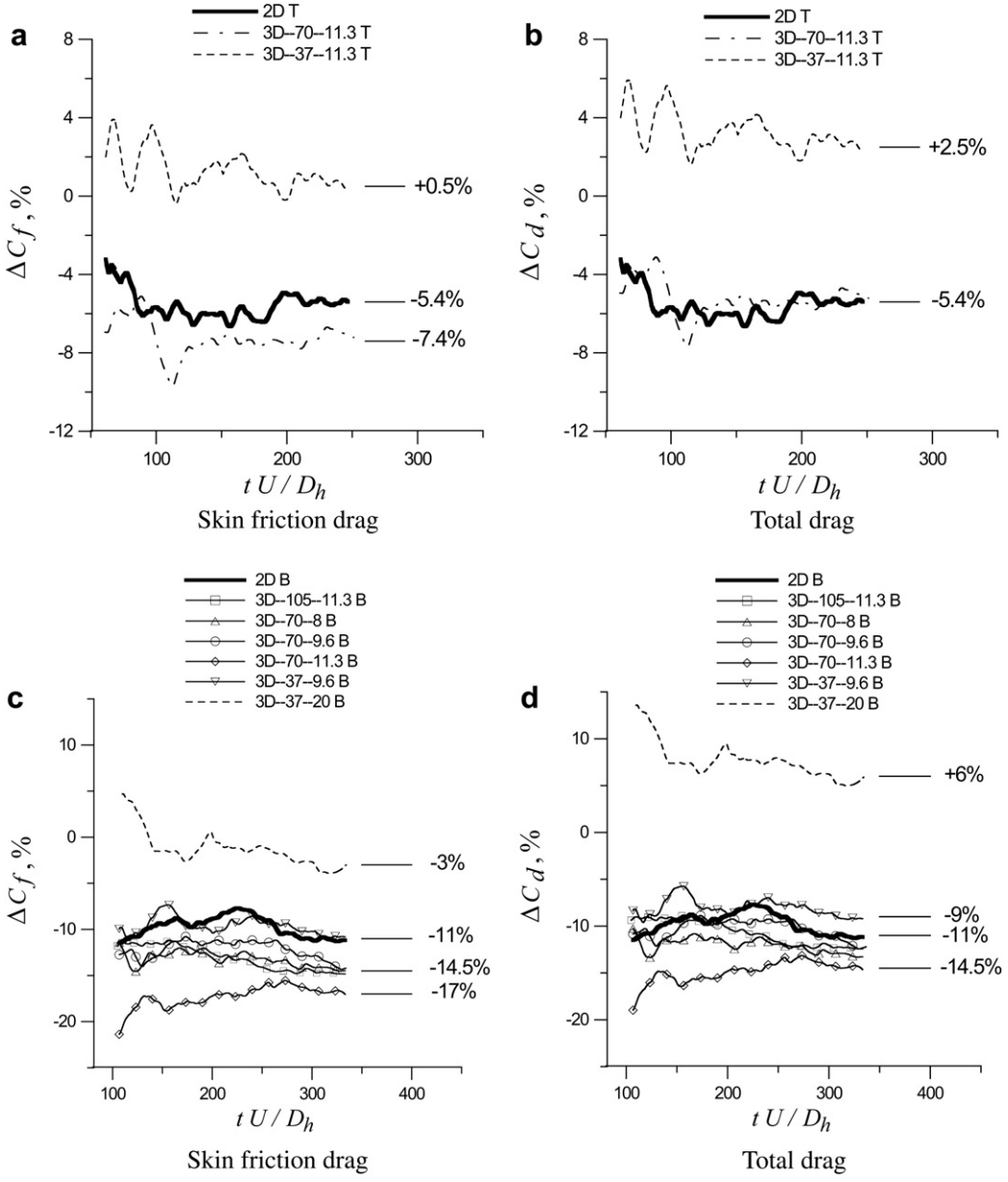

Fig. 5 – Time history of drag modification. (a), (b): triangular structures; (c), (d): knife-blade structures.

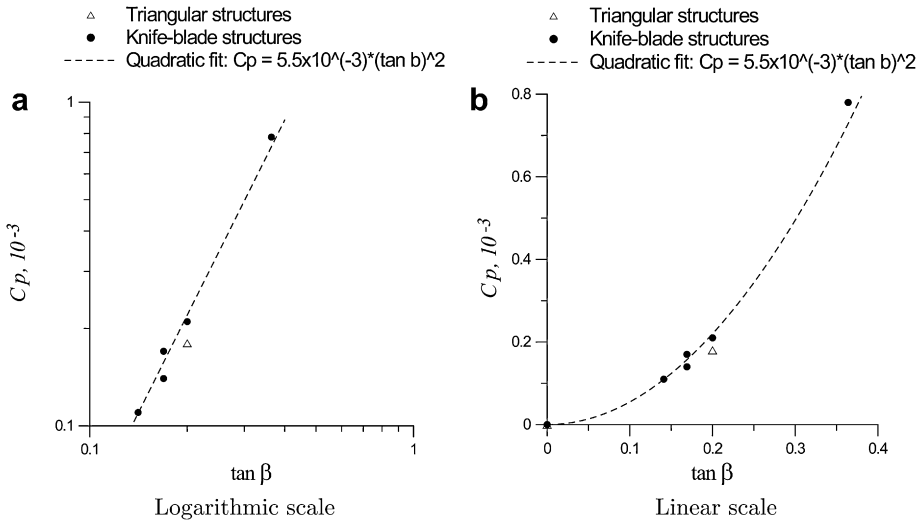

Fig. 6 – Pressure coefficient C_p versus the slope angle.

skin friction value can exceed that of a smooth wall. This behavior suggests that there exists an optimum value of excitation, ε_{opt}, which gives the maximum value of the skin friction reduction with respect to the smooth wall. The fact that the data for both triangular and knife-blade structures give a similar shape for the curve $\Delta C_f(\varepsilon)$ with approximately the same value for an optimum excitation is encouraging, see Fig. 7, and the present calculations suggest that the optimum excitation value is $\varepsilon_{opt} \sim 1 \times 10^{-4}$.

Expressing the excitation parameter ε (Eq. (12)) through $\tan\beta$ and λ^+ (using $T^+ = \lambda^+(Re_\tau/Re)$ and $\tan\beta = (2\,\pi\,a^+)/\lambda^+$) gives the following relation for the optimum structure shape

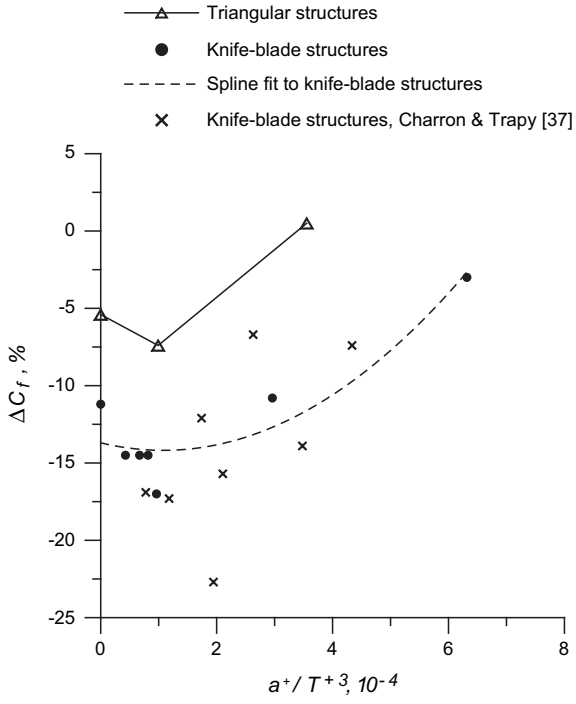

Fig. 7 – Skin friction modification ΔC_f versus the transverse excitation parameter ε.

$$\tan\beta = 2\pi\varepsilon_{opt}\left(\frac{Re_\tau}{Re}\right)^3 \lambda^{+2}. \tag{13}$$

Relation (13) is graphically visualized in Fig. 8, and the actual values of tan α and β for the calculated cases (Tables 2 and 3) are also included in the figure. It can be verified that the cases 3D–70–11.3 T and 3D–70–11.3 B both lie on the optimum curve, giving the maximum skin friction reduction (if compared to the other calculated triangular or knife-blade cases, respectively). Since the pressure drag increases quadratically with tan β (Eq. (11)), the objective for minimizing the total drag would be to choose parameters (β, λ^+) such that they lie on the optimum curve (13) but the angle β is as small as possible. Obviously, some restriction for the minimum effective angle β should exist, because without such a restriction the pair ($\beta = 0°$, $\lambda^+ = 0$) would be the optimum choice, which corresponds to the two-dimensional structures and clearly does not provide the optimum total drag value (see Table 7 and Fig. 5). It is known that the near-wall turbulence consists of coherent streamwise vortices and high- and low-speed streaks formed by the vortices [38]. The streamwise correlation length of the turbulence structures, i.e. the distance which the vortices travel before a breakdown, or the characteristics length of the low-speed streaks, L, is estimated to be about 1000 in wall units defined previously, i.e. $L^+ = L/u_\tau \sim 1000$ [38]. It is possible that if the oscillation wavelength λ^+ for the sinusoidal structures is made smaller than the streamwise turbulence correlation length L^+, the streamwise development of coherent motions in a turbulent boundary layer is affected. Since the streamwise coherent motions are believed to be responsible for the self-sustaining energy production cycle in a turbulent boundary layer [35], interference with their development might result in a different behavior of the near-wall turbulence, which might negatively effect skin friction reduction properties. This means that the effective skin friction reduction can not be obtained with the short structures (even if they satisfy the optimum condition (13)), making only the part of the optimum curve to the right of $\lambda^+ = 1000$ operational (see Fig. 8). This would limit the minimum effective wavelength to $\lambda^+ \sim 1000$ and the minimum effective angle to $\beta \sim 9°$ (corresponding to the intersection of the optimum curve with the

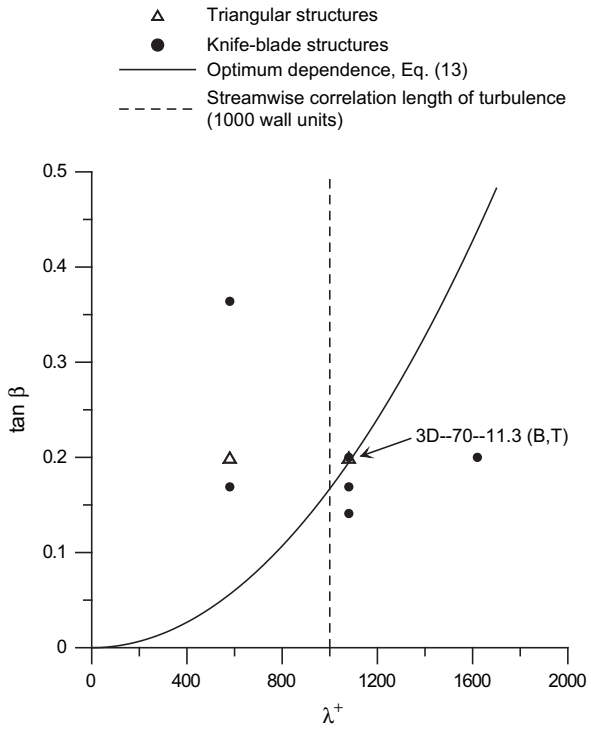

Fig. 8 – Dependence between tan β and λ^+ for the structured surfaces.

vertical line $\lambda^+ = 1000$), so that the pair ($\beta \sim 9^\circ$, $\lambda \sim 1000$) would under this reasoning correspond to the optimum three-dimensional structure shape. This conclusion has to be verified, however, by further computational and experimental investigations, since no compelling evidence exists that $\lambda^+ \sim L^+ \sim 1000$ is indeed the limiting wavelength and that the wavy structures with the shorter wavelengths will necessarily lose their efficiency in reducing the skin friction drag. Common sense suggests that such a minimum effective wavelength should exist, but in practice its value might be a fraction of the streamwise correlation length $L^+ = 1000$. Investigation of parameters lying on the optimum curve to the left of $\lambda^+ = 1000$ line is essential, especially since all the calculations done with the smaller wavelength $\lambda^+ = 580$ in this paper were significantly offset from the optimum curve (see Fig. 8). Therefore, there is no information on the performance of the surface structures with this short wavelength in a situation when the angle b is close to its optimum value.

7. Conclusions

In this paper, we investigated an ability of the structured surfaces added to the pipeline walls to reduce pressure losses with respect to smooth walls in order to cut costs during pipeline hydrogen transportation in large volumes. It was demonstrated earlier that conventional (two-dimensional) surface structures are capable of reducing pressure losses up to 10%, thus providing additional 5–6% cost benefits during a pipeline operation [18]. In this paper, we explored the recent development of three-dimensional (sinusoidal) structures [22] as a more efficient alternative to the two-dimensional structures in terms of the pressure loss reduction. One hidden drawback of the three-dimensional structures, missed in the previous investigations [22,33,37], is that, unlike the two-dimensional structures, the three-dimensional structures induce pressure drag in addition to skin friction drag. In this paper, we estimated both the skin friction and the pressure drag for various 3D structure configurations using reliable computational technique for turbulent flow calculations, Large Eddy Simulations. We were able to confirm that, even when the pressure drag is taken into account, the total drag is still significantly reduced by 3D structures compared to 2D structures (14.5% versus 11% reduction in the total drag reported for the most efficient 3D structure configuration of the ones investigated). We also performed a parametric study, and we found that the pressure drag scales as the square of the structure shape angle, $C_p \sim (\tan\beta)^2$. For the skin friction drag, an optimum curve has been derived in a two parameter space relating the optimum oscillation wavelength λ with the shape angle β. Minimizing the effective angle β while the two parameters (β and λ) lie on the optimum curve is therefore the objective to achieve the maximum total drag reduction. We suggested that the minimum effective angle would be limited, however, by the minimum effective wavelength λ, below which the spanwise flow oscillations would interfere negatively with the natural boundary layer turbulence structures, whose streamwise coherence length is $L^+ \sim 1000$. This interference might destroy the self-sustaining cycle of the turbulence energy production and thus change the boundary layer structure, thus resulting in a loss of skin friction reduction effectiveness. The exact value for the minimum effective wavelength λ is yet to be determined, however we can suggest from physical considerations that this value is somewhere below $\lambda^+ \sim 1000$.

Acknowledgements

This work was supported by Agence Nationale pour la Recherche (ANR) of France under the project PAN-H/READY (abbreviation for ‘‘National plan of action on hydrogen and fuel cells: prediction and reduction of pressure losses in hydrogen transport’’).

REFERENCES

[1] Gregory DP, Pangborn JP. Hydrogen energy. Annu Rev Energy 1976;1:279–310.
[2] Tellier C. Application of axial flow compressors for long distance pipeline transmission of hydrogen. Int J Hydrogen Energy 1981;6:413–22.
[3] Bulkcaen V. Energy losses in the transport in 4000 km pipelines of liqud hydrogen and oxygen derived from the splitting of water, and of liqud methane. Int J Hydrogen Energy 1992;17:613–22.
[4] Öney F, Veziro glu TN, Dülger Z. Evaluation of pipeline transportation of hydrogen and natural gas mixtures. Int J Hydrogen Energy 1994;19:813–22.

[5] Khristenko YA, Tomilin VP, Ryazhskih VI. Mathematical model for nonstationary regime of gaseous hydrogen outflow from vertical pipelines to atmosphere. Int J Hydrogen Energy 1999;24:1171–6.
[6] Jo Y-D, Ahn BJ. Analysis of hazard area associated with hydrogen gas transmission pipelines. Int J Hydrogen Energy 2006;31:2122–30.
[7] Wilkening H, Baraldi D. CFD modeling of accidental hydrogen release from pipelines. Int J Hydrogen Energy 2007;32:2206–15.
[8] Thompson AW, Bernstein IM. Selection of structural materials for hydoren pipelines and storage vessels. Int J Hydrogen Energy 1977;2:163–73.
[9] Capelle J, Gilgert J, Dmytrakh I, Pluvinage G. Sensitivity of pipelines with steel API X52 to hydrogen embrittlement. Int J Hydrogen Energy 2008;33:7630–41.
[10] Walters GA. Dynamic programming approach to the optimal design of tree-like networks. In: Proceedings of the international conference on optimization techniques and applications. Singapour, Singapore;1987. p. 487–96.
[11] Nie Ting Ze. Optimal lay-out of natural gas pipeline network. In: 23rd World gas conference. Amsterdam; 2006.
[12] Yang C, Ogden J. Determining the lowest-cost hydrogen delivery mode. Int J Hydrogen Energy 2007;32:268–86.
[13] Weng ZM, Chen DZ. Numerical method for computation of turbulent flow field of two-dimensional hydrogen-air mixing stream with detailed chemical reaction mechanism. Int J Hydrogen Energy 1988;13:355–62.
[14] Elaoud S, Hadj-Taieb E. Transient flow in pipelines of high-pressure hydrogen–natural gas mixtures. Int J Hydrogen Energy 2008;33:4824–32.
[15] Choi K-S. Near-wall structure of a turbulent boundary layer with riblets. J Fluid Mech 1998;208:417–58.
[16] Choi H, Moin P, Kim J. Direct numerical simulation of turbulent flow over riblets. J Fluid Mech 1993;255:503–39.
[17] Goldstein D, Handler R, Sirovich L. Direct numerical simulation of turbulent flow over modelled riblet covered surface. J Fluid Mech 1995;302:333–76.
[18] Charron Y, Mabile C. European program studies. Ways to fight internal pressure losses in gas lines. Pipeline Gas J June 2004;231(6):36–9.
[19] Walsh MJ, Lindemann AM. Optimization and application of riblets for turbulent drag reduction. AIAA Paper 84–0347. New York; 1984.
[20] Walsh J. Riblets. In: Bushnell DM, Heffner JN, editors. Viscous drag reduction in boundary layers. Washington, D.C.: AIAA; 1990. p. 203–61.
[21] Bechert DW, Bruse M, Hage W, Van Der Hoeven JGT, Hoppe G. Experiments on drag-reducing surfaces and their optimization with an adjustable geometry. J Fluid Mech 1997; 338:59–87.
[22] Charron Y, Lepesan E. Surface structurée tri dimensionnelle à onde transverse en vue d'une réduction de la traînée aérodynamique. Patent FR 2899 945; October, 2007.
[23] Jung WJ, Mangiavacchi N, Akhavan R. Suppression of turbulence in wall bounded flows by high-frequency spanwise oscillations. Phys Fluids 1992;8:1605–7.
[24] Laadhari F, Skandaji L, Morel R. Turbulence reduction in a boundary layer by a local spanwise oscillating surface. Phys Fluids 1994;6(10):3218–20.
[25] Choi K-S, DeBisschop JR, Clayton BR. Turbulent boundary-layer control by means of spanwise-wall oscillation. AIAA J 1998;36:1157.
[26] Schlichting H, Gersten K. Boundary layer theory. 8th revised and enlarged edition. Berlin, New York: Springer-Verlag; 2000.
[27] Blasius H. Das Ähnlichkeitsgesetz bei Reibungsvorgängen in Flüssigkeiten. Forschg Arb Ing-Wes; 1913. p. 131.
[28] Archambeau F, Méchitoua N, Sakiz M. Code_Saturne: a finite volume code for the computation of turbulent incompressible flows - industrial applications. Int J Fin Vol 2004:1.
[29] Gomez T, Flutet V, Sagaut P. Contribution of Reynolds stress distribution to the skin friction in compressible turbulent channel flows. Phys Rev E 2009;79:035301.
[30] Smagorinsky J. General circulation experiments with the primitive equations. J Mon Weather Rev 1963;91(3):99–164.
[31] Van Driest ER. Turbulent boundary layer in compressible fluids. J Aerospace Sci 1951;18(3):145–60.
[32] Peet Y, Sagaut P, Charron Y. Towards large eddy simulations of turbulent drag reduction using sinusoidal riblets, WSEAS Paper 565–355, 2007. In: 5th IASME/WSEAS international conference on fluid mechanics and aerodynamics. Vouliagmeni, Greece; 2007.
[33] Peet Y, Sagaut P, Charron Y. Turbulent drag reduction using sinusoidal riblets with triangular cross-section. AIAA Paper 2008–3745. In: 38th AIAA fluid dynamics conference and exhibit. Seattle, WA; 2008.
[34] Peet Y, Sagaut P. Theoretical prediction of turbulent skin friction on geometrically complex surfaces. Phys Fluids 2009; in press.
[35] Jiménez J, Moin P. The minimal flow unit in near-wall turbulence. J Fluid Mech 1991;225:213–40.
[36] Abe H, Kawamura H, Matsu Y. Direct numerical simulation of a fully developed turbulent channel flow with respect to Reynolds number dependence. ASME J Fluids Eng 2001; 123:382.
[37] Charron Y, Trapy J. Shape optimization of structured surfaces. Institut Français du Pétrole. JIP ICARE final Report; 2005.
[38] Robinson SK. Coherent motions in the turbulent boundary layer. Ann Rev Fluid Mech 1991;23:601–39.